2011

Oxygen Rich Titania: A Dopant Free, A Dopant Free, High Temperature Stable, and Visible-Light Active Anatase Photocatalyst

Vinodkumar Etacheri
Technological University Dublin

Michael Seery
Technological University Dublin, michael.seery@tudublin.ie

Steven Hinder
University of Surrey

Suresh Pillai
Technological University Dublin, suresh.pillai@tudublin.ie

Recommended Citation

Etacheri, V. et al. (2011) Oxygen Rich Titania: A Dopant Free, A Dopant Free, High Temperature Stable, and Visible-Light Active Anatase Photocatalyst, *Advanced Functional Materials*, 21, 2011, 3744-3752. doi:10.1002/adfm.201100301

FULL PAPER

Catalysis

V. Etacheri, M. K. Seery, S. J. Hinder, S. C. Pillai*.....x–xx

Oxygen Rich Titania: A Dopant Free, High Temperature Stable, and Visible-Light Active Anatase Photocatalyst

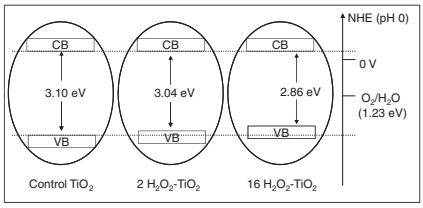

High temperature stable and visible-light active oxygen-rich titania nanoparticles are successfully synthesized through a peroxo-titania route. Increased Ti–O–Ti bond strength, oxygen excess defects and band gap narrowing are identified in these samples. It is proposed that the presence of oxygen excess defects is responsible for the high temperature stability and enhanced visible light photocatalytic activities.

ADVANCED FUNCTIONAL MATERIALS
www.afm-journal.de

Oxygen Rich Titania: A Dopant Free, High Temperature Stable, and Visible-Light Active Anatase Photocatalyst

*Vinodkumar Etacheri, Michael K. Seery, Steven J. Hinder, and Suresh C. Pillai**

The simultaneous existence of visible light photocatalytic activity and high temperature anatase phase stability up to 900 °C in undoped TiO_2 is reported for the first time. These properties are achieved by the in-situ generation of oxygen through the thermal decomposition of peroxo-titania complex (formed by the precursor modification with H_2O_2). Titania containing the highest amount of oxygen (16 H_2O_2-TiO_2) retains 100% anatase phase even at 900 °C, where as the control sample exists as 100% rutile at this temperature. The same composition exhibits a six-fold and two-fold increase in visible light photocatalytic activities in comparison to the control sample and the standard photocatalyst Degussa P-25 respectively. Among the various parameters affecting the photocatalytic action, such as band gap narrowing, textural properties, crystallite size, and anatase phase stability, band gap narrowing was identified as the major factor responsible for the visible light photocatalytic activity. Increased Ti–O–Ti bond strength and upward shifting of the valence band (VB) maximum, which is responsible for the high temperature stability and visible light activity respectively, are identified from FT–IR, XPS, and photoluminescence (PL) spectroscopic studies. It is therefore proposed that the oxygen excess defects present in these titania samples are responsible for the high temperature stability and enhanced visible light photocatalytic activities.

1. Introduction

Nano-sized titania find extensive applications in the area of solar cells, photocatalysts, pigments, water and air purification, electronic materials, cancer therapy, and self cleaning antibacterial materials.[1–11] The widespread applications of titanium dioxide in comparison to other semiconductor nanoparticles arise from the high redox potential, chemical stability, inexpensiveness, and non-toxicity. Among the three polymorphs of titania, anatase phase is reported as the most photocatalytically active because of its higher charge-carrier mobility and an increased density of surface hydroxyls.[12–14] On the other hand, rutile phase is found to be less active and photocatalytic activity of brookite phase is seldom investigated.[15] Photocatalytic activity of titania depends on various factors such as phase purity, surface area, crystallite size, quantity and nature of dopants, method of preparation and the anatase/rutile ratio.[16–18]

The most photocatalytically active anatase phase is metastable and irreversibly converted to the lesser photocatalytically active rutile at a temperature range of 600–700 °C.[3] This limits the use of titania photocatalysts for the high temperature (≥800 °C) applications (e.g., ceramic based building materials). Therefore, the development of an anatase photocatalyst stable up to the processing temperature of the substrate is one of the major challenges in ceramic industries.[3,19,20] Uses of various cationic metal dopants (e.g. Al, Si, Ni, Ce, etc.) were reported by previous researchers for extending the anatase to rutile transformation (ART) to temperatures above 700 °C.[21–26] Formation of secondary impurities (e.g. Al_2TiO_5, $NiTiO_3$, $CeTi_4O_{24}$, $Ce_2Ti_2O_7$, etc.) at high temperature and a consequent decrease in the photocatalytic activity are the main disadvantages of this technique.[3,27] In addition, cationic doping also deteriorates the photocatalytic activity through the generation of charge carrier recombination centres.[10,28] High temperature stabilization of anatase phase through precursor modification and non-metallic doping were also reported recently.[3,27,29–31] Excess anions doping was also found to be reducing the photocatalytic activity through lowering the band gap. Moreover, anion doping (N, C, S, etc.) promotes the formation of oxygen vacancies, which decreases photocatalytic activity by enhancing electron-hole recombination.[32] Recently, phosphorus doping was also reported to be associated with the formation of a new secondary phase TiP_2O_7 at higher temperatures.[33] The calcination atmosphere was found to have a significant effect on anatase to rutile transformation. Introduction of oxygen gas during the annealing process showed

V. Etacheri, Dr. S. C. Pillai
Centre for Research in Engineering Surface Technology (CREST)
FOCAS Institute
Dublin Institute of Technology
Camden Row, Dublin 8, Ireland
E-mail: suresh.pillai@dit.ie
Dr. M. K. Seery
School of Chemical and Pharmaceutical Sciences
Dublin Institute of Technology
Kevin Street, Dublin 8, Ireland
Dr. S. J. Hinder
The Surface Analysis Laboratory
Faculty of Engineering and Physical Sciences
University of Surrey
Guildford, Surrey, GU2 7XH, United Kingdom

DOI: 10.1002/adfm.201100301

an anatase stabilizing effect; on the other hand, employing a reducing environment (e.g., hydrogen gas) accelerated the transformation to rutile.[34,35]

Though the anatase titania is highly photocatalytically active, its wide band gap (3.2 eV) confines its application to the UV region ($\lambda \leq 390$ nm), which means that the conventional photocatalysts can just utilise 5% of the solar energy.[36] This has a significant impact on the commercial application of these materials. In order to utilize irradiation from sunlight or from artificial room light sources more effectively, the development of visible light active titania is necessary. Transition metal and anionic doping were employed for the visible light activation of titania.[37–40] However, as mentioned previously, these methods have the drawbacks of secondary phase and oxygen vacancy formation respectively.[10,28,32] Sensitization using an organic dye was another technique employed for visible light activation, which results in the degradation of the dye itself.[41] Reduced forms of TiO_2, which introduces localized oxygen vacancies were also reported for visible light applications.[39,42] Visible light activity and the high temperature stability of these catalysts were not sufficient for real-life applications. Under these circumstances, it is necessary to develop an effective method for the synthesis of high temperature stable and visible-light active anatase photocatalyst without the formation of secondary phases and oxygen vacancies. To the best of our knowledge, there are no systematic studies reported for the synthesis of high temperature stable and visible light active anatase titania without using any dopants. Here, we report a straightforward aqueous peroxo-titania route for the synthesis of high temperature stable and visible-light active, oxygen rich, anatase phase titanium dioxide. In this method, amorphous titanium dioxide reacts with hydrogen peroxide to form an orange coloured peroxo-titania complex, which on calcination above 400 °C forms nanocrystalline titania.[43–46] The high temperature stability and band gap of the resulting titania was tuned by varying the molar ratio of hydrogen peroxide. Unlike the conventional sol–gel process, the present method proceeds through an environmentally benign aqueous solution phase.

2. Results and Discussion

2.1. Formation of Oxygen Rich Anatase Nanoparticles

High temperature stable and visible light active oxygen rich titania were obtained through an aqueous peroxo-titania route. FT–IR spectra of the hydrogen peroxide modified (oxygen rich) and control titania xerogel (**Figure 1**) verified the formation of a peroxo-titania complex by the reaction between amorphous titanium dioxide and H_2O_2. For these complexes, peaks corresponding to O–O, Ti–O–O and Ti–O–Ti bonds were identified at 904 cm^{-1}, 686 cm^{-1} and 530 cm^{-1} respectively.[47,48] These peaks were appeared at higher frequencies for the peroxo-titania complexes containing higher H_2O_2 concentration (for example 16:1 H_2O_2-TiO_2). No such peaks representing the formation of a peroxo-titania complex was observed for the control xerogel and only Ti–O–Ti bonds were observed at 590 cm^{-1}. In addition, the peaks corresponding to adsorbed water and NH_3 molecules were appeared at 1623 cm^{-1} and 1400 cm^{-1} respectively.[49] X-ray diffraction patterns of titania obtained at different calcination temperatures established the high temperature stability of oxygen rich anatase titania in comparison to the control sample. Both oxygen rich and control titania samples obtained at 600 and 700 °C were pure anatase (Figure S1). Whereas at a higher calcination temperature of 900 °C, the control converted to 100% rutile and oxygen rich $16H_2O_2$-TiO_2 remains as 100% anatase (**Figure 2**). All other H_2O_2 modified compositions exists as anatase-rutile mixtures at this temperature.

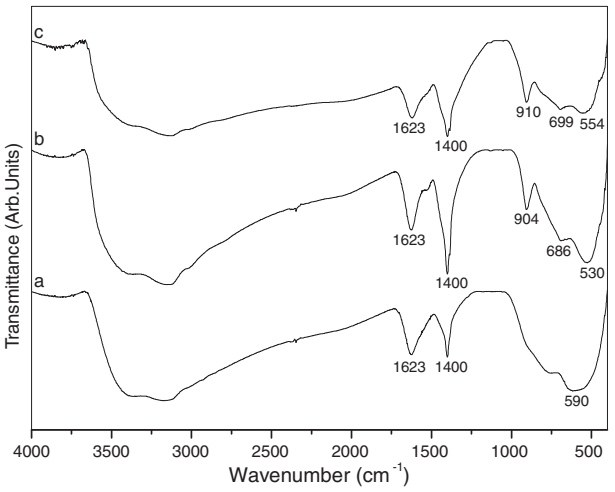

Figure 1. FT-IR Spectrum of 100 °C dried titania precursor: a) control xerogel, b) $2H_2O_2$-TiO_2 xerogel, c) $16H_2O_2$-TiO_2 xerogel

The crystallite sizes of these oxygen rich titanium dioxide were highly dependent on the Ti:H_2O_2 molar ratio. For example, at a calcination temperature of 900 °C, the control sample has a crystallite size of 73 ± 3 nm, whereas a smaller crystallite size of 50 ± 3 nm was observed for $16H_2O_2$-TiO_2 (Figure S2). In addition, a decrease in c/a ratio associated with an increase of the lattice parameter a was identified with an increase of oxygen content

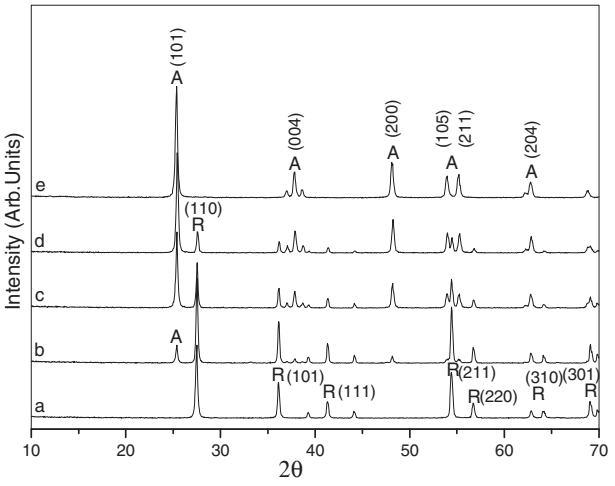

Figure 2. XRD patterns of TiO2 calcined at 900 °C: a) control TiO_2, b) $2H_2O_2$-TiO_2. (c) $4H_2O_2$-TiO_2 (d) $8H_2O_2$-TiO2 (e) $16H_2O_2$-TiO_2 (A = anatase; R = rutile)

Table 1. Lattice parameters of TiO_2 samples prepared at 600 °C.

Composition	*a* (Å)	*c* (Å)	*c/a*
Control-600	3.7699	9.4738	2.5130
$2H_2O_2$-TiO_2-600	3.7765	9.4738	2.5086
$16H_2O_2$-TiO_2-600	3.7796	9.4738	2.5066

Table 2. O_2:Ti ratio of the control and H_2O_2 modified TiO_2.

Composition	Ti 2p [At.%]	O 1s [At.%]	O_2:Ti
Control-TiO_2-600 °C	23.61	59.13	2.50
2 H_2O_2-TiO_2-600 °C	24.59	62.91	2.56
16 H_2O_2-TiO_2-600 °C	24.94	66.50	2.67
Control-TiO_2-700 °C	23.53	59.10	2.51
2 H_2O_2-TiO_2-700 °C	22.56	57.56	2.54
16 H_2O_2-TiO_2-700 °C	24.01	61.26	2.56
Control-TiO_2-900 °C	23.41	58.01	2.48
2 H_2O_2-TiO_2-900 °C	23.78	59.45	2.50
16 H_2O_2-TiO_2-900 °C	24.12	61.02	2.53

(**Table 1**). The variation of lattice parameters can be explained on the basis of defect concentration. Calcination of titania in an oxygen rich atmosphere (due to an in situ formation of oxygen) results in the formation of interstitial oxygen, which was observed from an FT–IR peak at 1107 cm^{-1}.[50] These interstitial O bind with an O on the lattice site, forming a substitutional O_2 molecule,[51] which results in the slight outward movement of the neighbouring Ti atoms and a consequent increase in lattice parameters. Increase of lattice parameters with an increase of H_2O_2 concentration may be due to the formation of more interstitial oxygen during the heat treatment. High temperature stability of the oxygen rich titania up to 900 °C as identified from the XRD results were further confirmed using the more surface-sensitive Raman spectroscopic technique (Figure S3).[52] The Raman active modes for anatase (A_{1g} + $2B_{1g}$ + $3E_g$ at 147, 197, 396, 515 and 638 cm^{-1}) and rutile (A_{1g} +B_{1g} + B_{2g} + E_g at 144, 238, 447 and 611 cm^{-1}) were used as fingerprints.[53–55]

Modification of the titania precursors with H_2O_2 results in a significant increase in the oxygen content of the titania and 16 H_2O_2-TiO_2 has the highest amount of oxygen at various calcination temperatures (**Table 2**). X-ray photoelectron spectroscopy (XPS) results demonstrated increased Ti $2p_{3/2}$ (Ti–O) binding energies for oxygen rich samples in comparison to the control sample. For example, at a calcination temperature of 600 °C, Ti $2p_{3/2}$ binding energies for the control, 2 H_2O_2-TiO_2 and 16 H_2O_2-TiO_2 were 458.78, 459, and 459.11 eV respectively (**Figure 3**A). Similar increase in O 1s binding energies were also identified for the oxygen rich compositions (Figure 3B). Increased Ti $2p_{3/2}$ and O 1s binding energies were also identified for these oxygen rich samples calcined up to 900 °C (Figure S4 and S5). Lower Ti $2p_{3/2}$ and O 1s binding energies for control TiO_2 is a direct measure of the lowering of valence state level of Ti^{4+} to Ti^{3+} and Ti^{2+} due to the formation of oxygen vacancies at higher calcination temperatures.[54,56] Such a binding energy decrease points towards the existence of oxygen vacancies and Ti^{3+} in control sample and only Ti^{4+} in oxygen rich TiO_2. The crystallite sizes of control and oxygen rich titania obtained from HR-TEM analysis were also consistent with the average crystallite size obtained from the XRD analysis. For instance, the average crystallite size of 75 ± 3 nm and 50 ± 3 nm were observed for control and 16 H_2O_2-TiO_2 formed at 900 °C (**Figure 4**). Thus it is evident from the above observations that an increase of O_2:Ti Ratio, Ti $2p_{3/2}$, and O 1s binding energies together with FT–IR and XRD results established the formation of oxygen rich anatase titania nanoparticles as a result of precursor modification with H_2O_2.

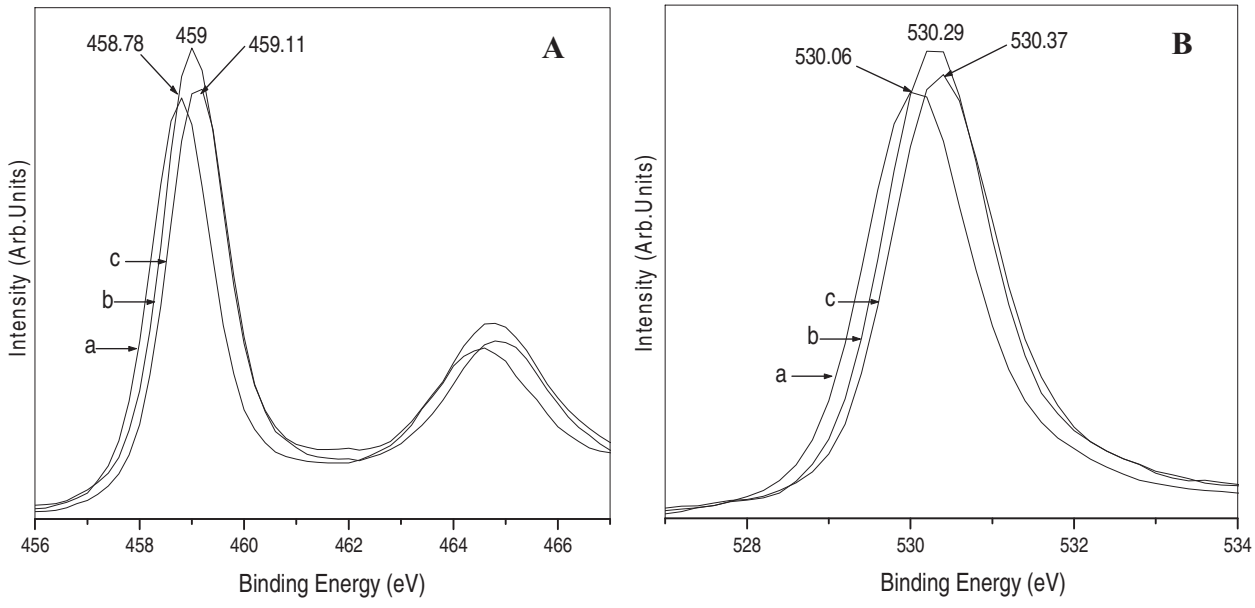

Figure 3. A) Ti 2p and B) O 1s - XPS peaks of TiO_2 calcined at 600 °C for (a) control TiO_2 (b) 2 H_2O_2-TiO_2 (c) 16 H_2O_2-TiO_2.

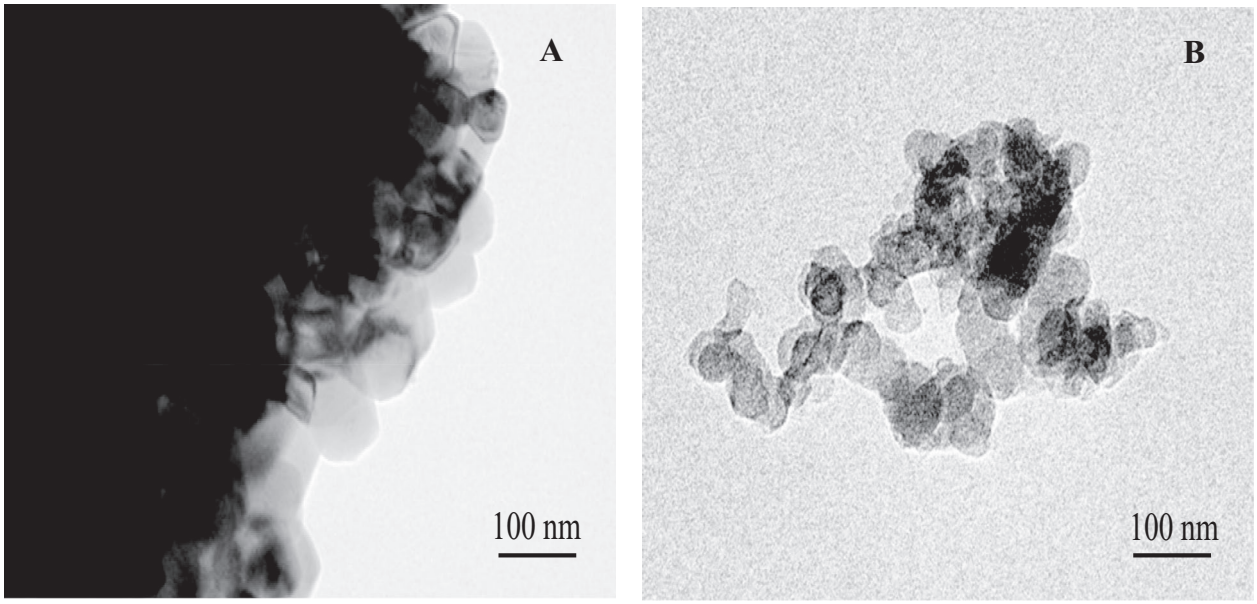

Figure 4. Transmission electron micrograph of A) Control TiO_2-900, B) 16 H_2O_2-TiO_2-900.

2.2. High Temperature Stability of Oxygen Rich Titania

The process of anatase to rutile phase transformation involves breaking of only two of the six Ti–O bonds in anatase.[35] This usually commences with oxygen vacancy formation, which accelerates the Ti–O bond breaking and phase transition associated with crystallite growth. Under normal synthesis conditions, high temperature treatment of titania always results in the formation of oxygen vacancies.[32,34,35] During the high temperature treatment, the Ti–O–Ti network weakens and this facilitates the Ti–O bond breaking and a consequent structural rearrangement to a thermodynamically stable rutile phase.[35] An increased Ti–O–Ti bond strength with an increase of oxygen content was also observed from the FT-IR spectra (Figure S6). This can be attributed to the in situ generation of oxygen due to the thermal decomposition of peroxo–titania complex, which can hinder the oxygen vacancy formation and retains the strength of Ti–O–Ti network. These stronger Ti–O–Ti bonds hinder the Ti–O bond cleavage at higher calcination temperatures and results in anatase phase stabilization and slow crystallite growth. Increased anatase phase stability with an increase of H_2O_2 concentration (oxygen content) may be due to the formation of higher amounts oxygen gas during heat treatment and stronger Ti–O–Ti bonds, which was also confirmed from the XPS and FT-IR results respectively.

Nitrogen isotherms of both control and oxygen rich titania (Figure S7) showed type IV characteristics with H1 type (cylindrical shape) of hysteresis.[57] However, with an increase of oxygen content, the steepness of the hysteresis loop increased and the end of the hysteresis loop shifted towards higher relative pressure (P/P_0), which represent their superior textural properties. For example, the thermally most stable oxygen rich composition (16 H_2O_2-TiO_2) calcined at 900 °C has a 78-fold increases in surface area, a 5-fold increase in pore diameter and the pore volume in comparison to the control sample calcined at the same temperature (Table S1). The increased pore diameter observed for both control and oxygen rich compositions on increasing the calcination temperature may be due to the formation of interstitial pores associated with excessive grain growth at high temperatures.[57] Stronger Ti–O–Ti bonds associated with smaller crystallite sizes of oxygen rich titania may be the vital reasons behind these improved textural properties.

2.3. Electronic Structure of Oxygen Rich Titania

High temperature stable oxygen rich titania samples have significant smaller band gap values at all calcination temperatures in contrast to the control sample. This narrowing effect was also found to be proportional to the amount of H_2O_2 (O_2:Ti ratio) used for precursor modification (**Table 3**). For example, the control sample at 700 °C has a band gap of 3.10 eV, whereas a gradual band gap narrowing was identified on increasing the oxygen content and the smallest band gap of 2.86 eV was obtained for 16 H_2O_2-TiO_2 (**Figure 5**A). Similar band gap narrowing was observed for these H_2O_2 modified

Table 3. Band gap values of TiO_2 calcined at various temperatures.

Composition	Band gap (eV) 600 °C	Band gap (eV) 700 °C	Band gap (eV) 800 °C	Band gap (eV) 900 °C
Control TiO_2	3.15	3.10	2.96	2.92
2 H_2O_2-TiO_2	3.12	3.04	2.98	2.94
4 H_2O_2-TiO_2	3.10	2.98	2.87	2.85
8 H_2O_2-TiO_2	3.08	2.94	2.83	2.83
16 H_2O_2-TiO_2	3.00	2.86	2.80	2.82

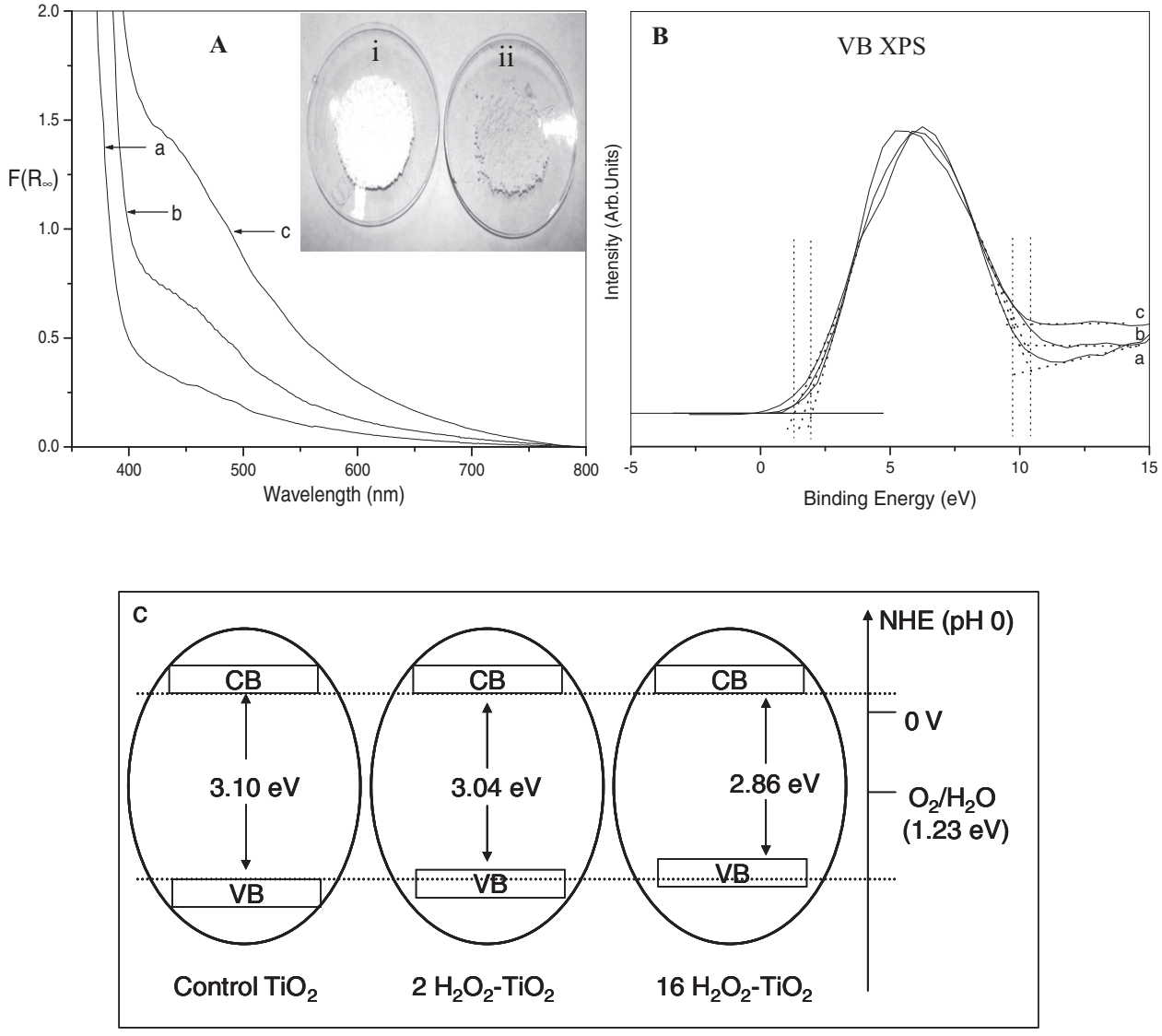

Figure 5. A) Optical absorption spectra of TiO_2 calcined at 700 °C: a) control TiO_2, b) 2 H_2O_2-TiO_2, c) 16 H_2O_2-TiO_2. Inset: i) control TiO_2 ii) 16 H_2O_2-TiO_2. B) Valence band XPS spectrum of TiO_2 calcined at 700 °C: a) control TiO_2, b) 2 H_2O_2-TiO_2, c) 16 H_2O_2-TiO_2. C) Mechanism of band gap narrowing.

titania at all calcination temperatures. It was also noticed that all the oxygen rich compositions were light yellow coloured, whereas the control sample has pure white colour (Figure 5A inset). Since all titania samples exist as pure anatase at 600 and 700 °C, the band gap narrowing due to rutile phase formation can be excluded. Two possible reasons behind band gap narrowing are the lattice parameter variations and valence band modification resulting from oxygen excess defects. Lattice parameter is an important factor affecting the band gap and decreases in band gap values were observed with an increase of lattice parameters for III–V semiconductors.[58] With the aid of *ab-initio* calculations, Wunderlich *et al.* also reported the band gap narrowing associated with lattice parameter increase for TiO_2 thin films.[59] As discussed previously, the in situ generation of oxygen from the peroxo–titania complex results in the formation of titania containing interstitial oxygen excess defects. These defects interact with lattice oxygen atoms, which results in an increase of lattice parameters and a consequent band gap lowering.[51,59]

In order to further investigate the band gap narrowing phenomenon, the valence band (VB) XPS patterns of both control and oxygen rich titania were recorded (Figure 5B), which reveal the shifting of the VB maximum of oxygen rich titania to lower binding energies. For instance, the VB maximum of control, 2 H_2O_2-TiO_2 and 16 H_2O_2-TiO_2 obtained at 700 °C appeared at 1.95 eV, 1.88 eV, and 1.70 eV respectively. The VB maximum of 1.95 eV obtained for the control titania was identical to those obtained by previous researchers for pure anatase phase titania.[60,61] In addition to this, equal width of their valence band of about 8.5 eV represent almost similar mobilities of the photo-generated charge carriers.[60,61] Because the band gap of these control TiO_2, 2 H_2O_2-TiO_2, and 16 H_2O_2-TiO_2 are 3.10 eV, 3.04 eV, and 2.86 eV from the UV/Vis absorption spectrum, the conduction band minimum for all would occur

at about –1.15 eV. Thus, the upward shifting of the VB maximum for oxygen rich titania is identified as another crucial reason responsible for efficient visible light absorption. Typical band gap structures of control and oxygen rich titania samples obtained at 700 °C are represented in Figure 5C.

The band gap narrowing due to valance band modifications were also supported by the Photoluminescence (PL) results. The oxygen rich titania samples were less luminescent in comparison to the control sample at all calcination temperatures (Figure S8). which can be attributed to the increased radiative electron hole recombination rate due to the presence of oxygen vacancies present in the control sample.[62–64] On the other hand, the possibility of oxygen vacancy formation and consequent electron-hole recombination are less for oxygen rich titania. In addition, excess oxygen present in titania can also act as an electron scavenger, which reduces the luminescence.[65] The anatase titania samples calcined at 600 °C has two main PL bands having different intensities (Figure S8). For the control sample, the most intense emission peak at 3.2 eV, which corresponds to the band gap energy of anatase titania results from the indirect transition $X_{1b} \rightarrow \Gamma_3$ (where X and Γ represents the edge and centre of the Brillouin zone respectively).[66] The less intense band at 3 eV represents two nearly degenerate indirect transitions $\Gamma_{1b} \rightarrow X_{2b}/X_{1a}$.[66,67] In contrast, the 3 eV peak was the most intense for all oxygen rich samples and its relative intensity increases with an increase of O_2:Ti ratio. This indicates an increased de-excitation of photo-excited electrons through $\Gamma_{1b} \rightarrow X_{2b}/X_{1a}$ transition. The conduction and valence bands of titania are derived mainly from the Ti-3d and O-2p states respectively.[64,66,68] Since the X_{2b}/X_{1a} are composed of O-2p states, the intensity reversal must be related to valence band modifications. It is also reported that oxygen vacancies and excess defects in TiO_2 results in the CB and VB modification respectively.[32,42] Previous researchers also identified similar PL peak intensity reversal associated with VB modification for ZnO containing oxygen excess defects.[69–72] These reports by previous researchers and our PL spectroscopic results well support the band gap narrowing due to valence band modification.

2.4. Visible Light Photocatalytic Activity Evaluation

Oxygen rich titania compositions exhibited enhanced visible light photocatalytic activities in comparison to the control sample, and the photocatalytic activities were also found to be a function of the O_2:Ti ratio (Table S2). For example, at calcination temperatures of 600, the control sample was the least active, and 16 H_2O_2-TiO_2 the most active photocatalyst. Calculated rate constant for these compositions were 0.0025 min^{-1} and 0.0163 min^{-1} respectively. The photocatalytic activities were found to be decreasing with an increase of calcination temperature, which can be due to the decrease in the surface area. At the highest calcination temperature of 900 °C, the most oxygen rich and thermally stable sample has also showed the highest photocatalytically activity (**Figure 6**). The photocatalytic activity of this sample was almost six-fold and two-fold higher in comparison to the control titania prepared under similar conditions and the standard photocatalyst Degussa P-25 respectively (**Figure 7**). Increased blue shift observed for the UV/Vis spectra of methylene blue during the degradation with oxygen rich titania indicates faster dye degradation through N-demethylation mechanism.[73,74]

The superior visible light photocatalytic activity of oxygen rich titania samples can be explained on the basis of high temperature anatase phase stability, oxygen vacancy formations, superior textural properties, and band gap narrowing. The anatase phase retention may be the key reason behind the increased photocatalytic activities of oxygen rich samples at high temperatures (for example, 900 °C). The excess oxygen vacancies created during the heat treatment of titania act as electron-hole

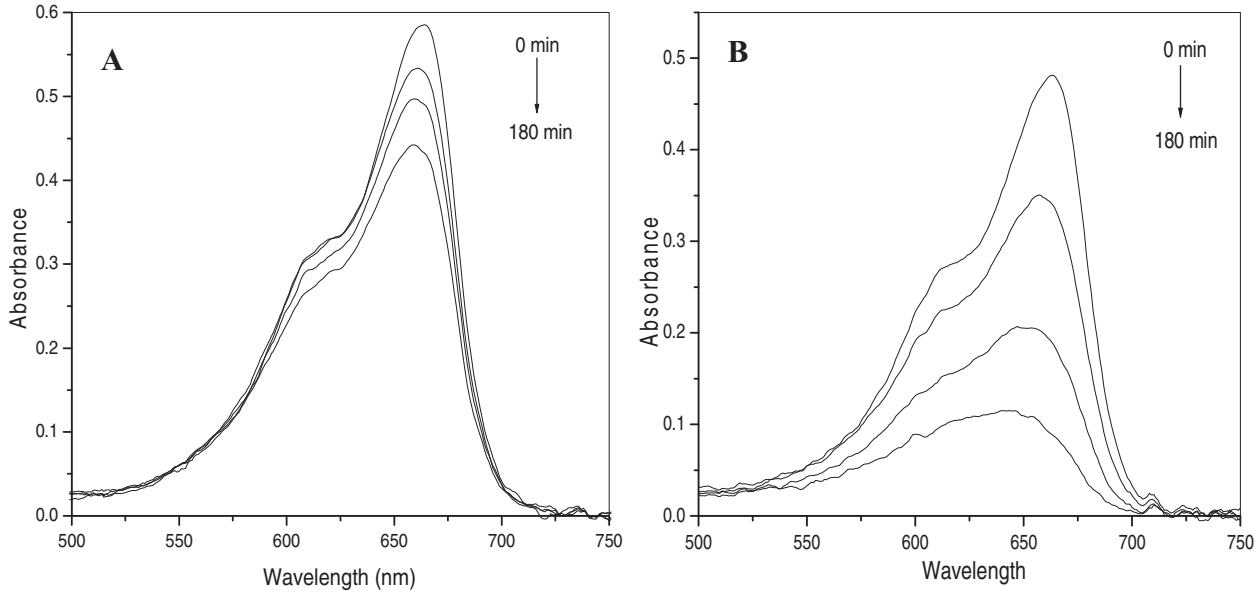

Figure 6. Absorption spectra of visible light induced methylene blue degradation using: A) control TiO_2-900, B) 16 H_2O_2-TiO_2-900.

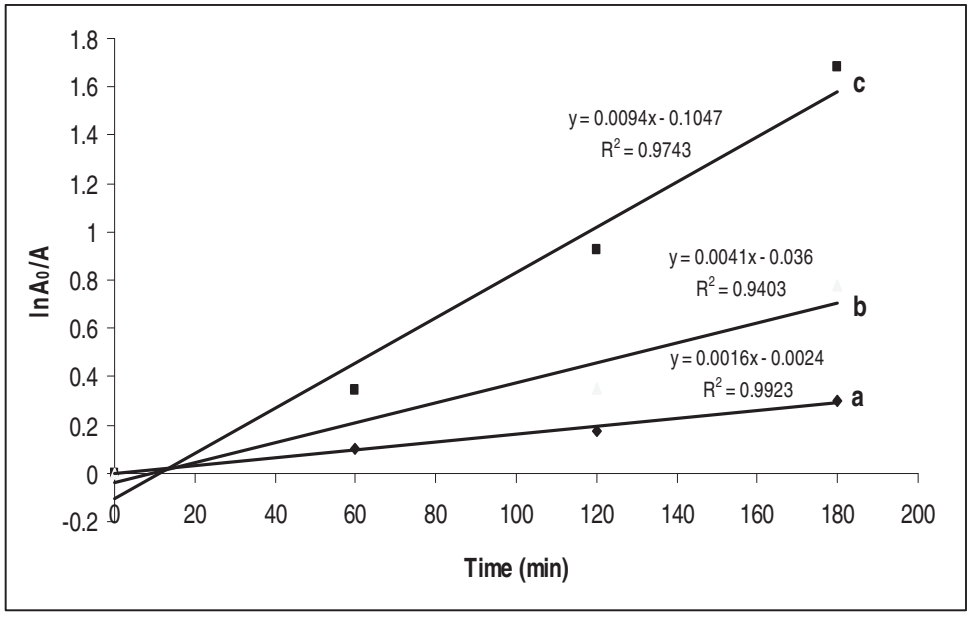

Figure 7. Kinetic study of a) control TiO_2-900, b) Degussa P-25, c) 16 H_2O_2-TiO_2-900.

recombination centers[32,62,63] and thereby decrease the overall photocatalytic efficiency. On heat treatment, the control titania sample becomes non-stoichiometric through oxygen vacancy formation,[35,62] whereas the H_2O_2 modified compositions were found to be oxygen rich. Thus, a fast electron-hole recombination was expected in control titania in comparison to the H_2O_2 modified compositions. This can be considered as another key factor behind the enhanced photocatalytic activities of oxygen rich titania. Efficiency of a visible light photocatalyst highly depends on its ability to absorb and utilize visible light.[2,40,75,76] The enhanced visible light absorption and photocatalytic activity observed for titania with an increase of oxygen content points towards the fact that the efficient visible light absorption is also responsible for their high photocatalytic activity.

Since the oxygen rich titania at all calcination temperatures possess enhanced textural properties associated with smaller crystallite size, band gap narrowing, and anatase phase stability, it is necessary to distinguish the real factor responsible for enhanced visible light photocatalytic activity. For this, the photocatalytic activity of oxygen rich anatase phase titania (16 H_2O_2-TiO_2-600) having a band gap of 3.00 eV and surface area 58 $m^2\ g^{-1}$ was compared with sol–gel synthesized nano sized (12 nm) anatase phase titania having 134 $m^2\ g^{-1}$ surface area and band gap of 3.2 eV. This study revealed almost four-fold higher photocatalytic activity of oxygen rich titania in comparison to sol–gel titania (Figure S9). In addition to this we also reported the excellent visible light photocatalytic activity of N-doped anatase rutile heterojunctions having low surface area.[2] This comparison provides the evidence that though the photocatalyst has superior textural properties, smaller crystallite size and anatase phase stability, narrow band gap is the primary factor in deciding the visible light photocatalytic efficiency. On the other hand, for a series of visible light absorbing titania photocatalysts, enhanced textural properties, nanosized nature and anatase phase stability may act as secondary factors for increasing the activity.

3. Conclusions

High temperature stable and visible light active oxygen rich titania were fabricated through a peroxo–titania route. Both the high temperature stability and visible light photocatalytic activity were found to increase with an increase of O_2:Ti ratio. The most oxygen rich catalyst 16 H_2O_2-TiO_2 exists as 100% anatase even at 900 °C, where as the control sample was converted to 100% rutile at this temperature. Increase in the oxygen content results in lattice parameter variations and Ti–O–Ti bond strengthening. This bond strengthening mechanism was found to be responsible for extending the anatase phase stability up to 900 °C. The electronic structure analysis using UV–vis, PL and valence band XPS spectroscopic studies reveal the fact that the upward shifting of the valence band (VB) maximum were responsible for the band gap narrowing. The visible light photocatalytic activity of the most thermally stable and oxygen rich catalyst (16 H_2O_2-TiO_2-900) was almost six-fold and two-fold higher in comparison to the control sample and the standard photocatalyst Degussa P-25 respectively. Band gap narrowing was identified as the critical factor responsible for the visible light induced photocatalytic activities of these samples. The exceptionally higher anatase phase stability and visible light photocatalytic activity makes these oxygen rich titania a promising material for photocatalytic, self cleaning, and photovoltaic applications.

4. Experimental Section

Synthesis of Oxygen Rich Titania: All reagents were used without further purification. Titanium tetrachloride (Aldrich 99.9%) and hydrogen peroxide (Aldrich 30 wt.%) were used as the titania precursor and the chemical modifier respectively. In a typical synthesis of 1:2 H_2O_2 modified titania, titanium tetrachloride (5.5 mL) was added to 150 mL cold water (5 °C) to form titanium oxychloride. This solution

was converted to hydrated titanium dioxide by adjusting the pH to 7 using ammonium hydroxide (15 mL). The precipitate obtained was then repeatedly washed with deionised water to free chloride ions (tested with $AgNO_3$ solution) and stirred with hydrogen peroxide (10 mL) and deionised water (100 mL) for 1 h to form peroxo titanate complex. This solution, on heating at 50 °C for 2 h undergoes gelation, which was then dried in an air oven at 100 °C for 24 h. The xerogel obtained was then calcined at various temperatures in the range 600–1000 °C for 2 h at a heating rate of 10 °C/min. The amount of H_2O_2 used was varied from 10 to 80 mL in order to synthesize various modified titania samples (identified as 2 H_2O_2-TiO_2, 4 H_2O_2-TiO_2, 8 H_2O_2-TiO_2 and 16 H_2O_2-TiO_2 respectively after calcination). A control sample of TiO_2 was also prepared without using H_2O_2.

Characterization Techniques: A Perkin Elmer GX FT-IR spectrometer was used for recording the FT-IR spectra of xerogel and samples calcined at different temperatures. Transparent pellets were prepared by using a 4 mm die after uniformly mixing the samples with KBr and spectra were recorded in the range 4000–400 cm^{-1}. Differential scanning calorimetry (DSC) measurements were performed using a Rheometric Scientific DSC QC instrument. A small amount of the xerogel (5 mg) was heated from 25 °C to 600 °C at a constant heating rate of 10 °C min^{-1}. A Siemens D 500 X-ray diffractometer ($2\theta = 10–70°$) working with Cu-Kα radiation ($\lambda = 0.15418$ nm) was used for the crystal phase analysis of calcined samples. The amount of rutile phase in each sample was calculated using Spurr equation (Equation 1)

$$F_R = \frac{1}{1+0.8[I_A(101)/I_R(110)]} \quad (1)$$

where F_R is the amount of rutile in an anatase-rutile mixture, I_A (1 0 1) and I_R (1 1 0) are the anatase and rutile main peak intensities respectively. The scherrer equation (Equation 2) was used for the precise determination of anatase and rutile crystallite sizes in calcined titania samples.

$$\Phi = \frac{K\lambda}{\beta\cos\theta} \quad (2)$$

Where Φ is the crystallite size, λ is the wavelength of X-ray used; K is the shape factor, and β the full line width at the half-maximum height of the main intensity peak. The lattice parameters of anatase titania a and c were calculated from (101) and (200) reflections of the XRD pattern using equation 3. Where h, k, l are the miller indices and d is the spacing between the planes calculated from the 2θ angle by using Bragg's Law (Equation 4).

$$\frac{1}{d^2} = \frac{h^2+k^2}{a^2} + \frac{l^2}{c^2} \quad (3)$$

$$d = \frac{\lambda}{2\sin\theta} \quad (4)$$

A Dilor ISA Labram 1 B micro-Raman system equipped with a 514 nm Ar^+ ion laser was employed for recording the Raman spectra of calcined samples. A laser power of 3 mW was used for measurements in order to avoid sample burning. A Thermo Fisher Scientific (East Grinstead, UK) Theta Probe spectrometer using monochromatic Al-Kα radiation (photon energy 1486.6 eV) was used for the X-ray photoelectron spectroscopic (XPS) studies. A pass energy of 20 eV and a 0.2 eV step size were used for recording the high resolution Ti 2p and O 1s spectra. A low-energy electron flood gun was used for achieving charge compensation. The high-resolution core level spectra after the removal of a nonlinear Shirley background were used for quantitative surface chemical analysis. For all samples, the binding energies of all the elements present were determined by setting the CC/CH component of the C 1s peak at 285 eV. Absorption spectra of samples were recorded using a Perkin–Elmer Lambda 900 UV/Vis/NIR spectrometer equipped with an integrated sphere attachment using $BaSO_4$ as the reference. Titania samples were thoroughly mixed with KBr, and pellets were prepared with the help of a 4 mm die. The band gap values were calculated from these spectra by extrapolating the lower wavelength cutoff region. Room temperature photoluminescence spectra of samples were recorded using a Perkin-Elmer Luminescence Spectrometer (LS-55B) at an excitation wavelength of 260 nm. Powder samples were dispersed in deionised water (0.01 g in 100 mL) and sonicated for 30 min prior to the analysis.

Samples for transmission electron microscopy (TEM) were prepared by dispersing the powder samples in water followed by sonication for 30 min. A JEOL transmission electron microscope (JEM-2100 operating at an accelerating voltage of 200 kV) was used for the analysis of particle-loaded formvar-coated copper grids. All samples for surface area analysis were vacuum degassed at 300 °C for two hours. The nitrogen adsorption and desorption isotherms were collected using a Quantachrome 2000e surface area analyzer. The linear portion ($P/P_0 = 0.05–0.2$) of the Brunauer-Emmett-Teller (BET) model was used for the calculation of specific surface area. Pore diameter and volumes were calculated from the desorption branch of the Barret-Joyner-Halenda (BJH) model.

Visible Light Photocatalysis Study: Visible light photocatalytic activities of samples were analyzed through the methylene blue degradation technique.[73,74] A Q-Sun solar simulator and a primary blue filter (450 nm) were used for the visible light generation. In a typical photocatalytic degradation experiment, an aqueous solution of methylene blue (50 mL, 1×10^{-5} M) was mixed and stirred well with the catalyst (0.06 g) in a glass beaker (100 mL). The suspension thus obtained was kept under the dark for 30 min and then irradiated with visible light (0.68 W m^{-2}) with stirring. An air cooler and thermostat were connected to the solar simulator to maintain the temperature of suspension at 25 °C. Aliquots (3 mL) were withdrawn from the suspension under visible light irradiation at equal time intervals of 1 h and the absorption spectra were recorded using a Perkin-Elmer Lambda 900 UV/Vis/NIR spectrometer. Samples obtained at various calcination temperatures were also analyzed using the same method. The photocatalytic rate constant for methylene blue degradation (k) was determined from the first order plot (Equation 5).

$$\ln = \left(\frac{A_0}{A}\right) = kt \quad (5)$$

Where A_0 is the initial absorbance of methylene blue solution, A is absorbance after a time (t) and k is the first order rate constant. All photocatalytic degradation experiments were repeated three times. The calculated values of rate constants were within 5% error limit.

Supporting Information

Supporting Information is available from the Wiley Online Library or from the author.

Acknowledgements

The authors would like to thank Enterprise Ireland for funding (CFTD/06/IT/326 and ARE/2008/0005) and Dr. John Colreavy (Director, Centre for Research in Engineering Surface Technology) for supporting this study and for providing valuable suggestions.

Received: Feb 9, 2010
Revised: May 4, 2011
Published online:

[1] B. O'Regan, M. Grätzel, *Nature* **1991**, *353*, 737.
[2] V. Etacheri, M. K. Seery, S. J. Hinder, S. C. Pillai, *Chem. Mater.* **2010**, *22*, 3843.
[3] S. C. Pillai, P. Periyat, R. George, D. E. McCormack, M. K. Seery, H. Hayden, J. Colreavy, D. Corr, S. J. Hinder, *J. Phys. Chem. C* **2007**, *111*, 1605.
[4] J. Yuan, S. Tsujikawa, *J. Electrochem. Soc.* **1995**, *142*, 3444.
[5] H. Honda, A. Ishizaki, R. Soma, K. Hashimoto, A. Fujishima, *J. Illum. Eng. Soc.* **1998**, *42*.

[6] S. L. Pugh, J. T. Guthrie, *Dyes Pigm.* **2002**, *55*, 109.
[7] D. F. Ollis, H. Al-Ekabi, *Photocatalytic Purification and Treatment of Water and Air*, Elsevier, Amsterdam, **1993**.
[8] R. Cai, Y. Kubota, T. Shuin, H. Sakai, K. Hashimoto, A. Fujishima, *Cancer Res.* **1992**, *52*, 2346.
[9] A. Mills, S. K. Lee, *J. Photochem. Photobiol., A* **2002**, *152*, 233.
[10] W. Choi, A. Termin, M. R. Hoffmann, *J. Phys. Chem.* **1994**, *98*, 13669.
[11] P. V. Kamat, *J. Phys. Chem. C* **2007**, *111*, 2834.
[12] A. L. Linsebigler, G. Lu, Y. T. Yates, *Chem. Rev.* **1995**, *95*, 735.
[13] M. A. Fox, M. T. Dulay, *Chem. Rev.* **1993**, *93*, 341.
[14] M. Muruganandham, M. Swaminathan, *Sol. Energy Mater. Sol. Cells* **2004**, *81*, 439.
[15] T. Miyagi, M. Kamei, T. Mitsuhashi, T. Ishigaki, A. Yamazaki, *Chem. Phys. Lett.* **2004**, *390*, 399.
[16] L. Kavan, M. Grtzel, S. E. Gilbert, C. Klemenz, H. J. Scheel, *J. Am. Chem. Soc.* **1996**, *118*, 6716.
[17] M. Toyoda, Y. Nanbu, Y. Nakazawa, M. Hirano, M. Inagaki, *Appl. Catal., B* **2004**, *49*, 227.
[18] E. Beyers, P. Cool, E. F. Vansant, *J. Phys. Chem. B* **2005**, *109*, 10081.
[19] M. Machida, W. K. Norimoto, T. Kimura, *J. Am. Ceram. Soc.* **2005**, *88*, 95.
[20] A. Mills, S. K. Lee, *J. Photochem. Photobiol. A* **2006**, *182*, 181.
[21] D. J. Reidy, J. D. Holmes, M. A. Morris, *Ceram. Int.* **2006**, *32*, 235.
[22] Y. Miyake, H. Tada, *J. Chem. Eng. Jpn.* **2004**, *37*, 630.
[23] J. Nair, P. Nair, F. Mizukami, Y. Oosawa, T. Okubo, *Mater. Res. Bull.* **1999**, *34*, 1275.
[24] Y. Zhang, H. Zhang, Y. Xu, Y. Wang, *J. Mater. Chem.* **2003**, *13*, 2261.
[25] Y. Zhang, H. Zhang, Y. Xu, Y. Wang, *J. Solid State Chem.* **2004**, *177*, 3490.
[26] A. Burns, G. Hayes, W. Li, J. Hirvonen, J. D. Demaree, S. I. Shah, *Mater. Sci. Eng. B* **2004**, *111*, 150.
[27] Y. Lv, L. Yu, H. Huang, H. Liu, Y. Feng, *Appl. Surf. Sci.* **2009**, *255*, 9548.
[28] J. M. Hermann, J. Disdier, P. Pichat, *Chem. Phys. Lett.* **1984**, *108*, 618.
[29] P. Periyat, S. C. Pillai, D. E. McCormack, J. Colreavy, S. J. Hinder, *J. Phys. Chem. C* **2008**, *112*, 7644.
[30] K. Nukumizu, J. Nunoshige, T. Takata, J. N. Kondo, M. Hara, H. Kobayashi, K. Domen, *Chem. Lett.* **2003**, *32*, 196.
[31] M. Yan, F. Chen, J. Zhang, M. Anpo, *J. Phys. Chem. B* **2005**, *109*, 8673.
[32] G. R. Torres, T. Lindgren, J. Lu, C.-G. Granqvist, S.-E. Lindquist, *J. Phys. Chem. B* **2004**, *108*, 5995.
[33] H. F. Yu, *J. Phys. Chem. Solids.* **2007**, *68*, 600.
[34] Y. Lida, S. Ozaki, *J. Am. Ceram. Soc.* **1961**, *44*, 120.
[35] R. D. Shannon, *Chem. Abstr.* **1964**, *63*, 2468.
[36] Y. Q. Wang, X. J. Yu, D. Z. Sun, *J. Hazard. Mater.* **2007**, *144*, 328.
[37] M. G. Kang, N. G. Park, Y. J. Park, K. S. Ryu, S. H. Chang, *Sol. Energy Mater. Sol. Cells* **2003**, *75*, 475.
[38] U. Siemon, D. Bahnemann, J. J. Testa, D. Rodr´ıguez, M. I. Litter, N. Bruno, *J. Photochem. Photobiol. A-Chem.* **2002**, *148*, 247.
[39] I. Nakamura, N. Negishi, S. Kutsuna, T. Ihara, S. Sugihara, K. Takeuchi, *J. Mol. Catal. A: Chem.* **2000**, *161*, 205.
[40] R. Asahi, T. Morikawa, T. Ohwaki, K. Aoki, Y. Taga, *Science.* **2001**, *293*, 269.
[41] R. Abe, K. Sayama, H. Arakawa, *Chem. Phys. Lett.* **2002**, *362*, 441.
[42] I. Justicia, P. Ordejon, G. Canto, J. L. Mozos, J. Fraxedas, G. A. Battiston, R. Gerbasi, A. Figueras, *Adv. Mater.* **2002**, *14*, 1399.
[43] S. Ogata, Y. Matsui, *US patent 6344278 B1* **2002**.
[44] L. Ge, M. Xu, *J. Sol-Gel Sci. Technol.* **2007**, *43*, 1.
[45] L. Ge, M. X. Xu, M. Sun, *Mater. Lett.* **2006**, *60*, 287.
[46] K. Melghit, S. S. Al-Rabaniah, I. Al-Amri, *Ceram. Int.* **2008**, *34*, 479.
[47] T. Yoko, K. Kamiya, K. Tanaka, *J. Mater. Sci.* **1990**, *25*, 3922.
[48] M. R. Ayers, A. J. Hunt, *Mater. Lett.* **1998**, *34*, 290.
[49] S. Karuppuchamy, J. M. Jeong, *J. Oleo Sci.* **2006**, *55*, 263.
[50] G. He, Q. Fang, L. Zhu, M. Liu, L. Zhang, *Chem. Phys. Lett.* **2004**, *395*, 259.
[51] S. Na-Phattalung, M. F. Smith, K. Kim, M.-H. Du, S.-H. Wei, S. B. Zhang, S. Limpijumnong, *Phys. Rev. B: Condens. Matter* **2006**, *73*, 125205.
[52] K. Gao, *Physica B.* **2007**, *398*, 33.
[53] T. Ohsaka, F. Izumi, Y. Fujiki, *J. Raman Spectrosc.* **1978**, *7*, 321.
[54] H. Berger, H. Tang, F. Le´vy, *J. Cryst. Growth* **1993**, *130*, 108.
[55] H. Tang, K. Prasad, R. Sanjines, P. E. Schmid, F. Levy, *J. Appl. Phys.* **1994**, *75*, 2042.
[56] S. Hashimoto, A. Murata, T. Sakurada, A. Tanka, *J. Surf. Anal.* **2002**, *9*, 459.
[57] R. S. Nasar, M. Cerqueira, E. Longo, J. A. Varela, *Cerâmica* **2008**, *54*, 38.
[58] E. S. Machlin, *Materials Science in Microelectronics: The Effects of Structure on Properties in Thin Films*, Elsevier, **2006**.
[59] W. Wunderlich, L. Miao, M. Tanemura, S. Tanemura, P. Jin, K. Kaneko, A. Terai, N. Nabatova-Gabin, R. Belkada, *Int. J. Nanosci.* **2004**, *3*, 439.
[60] J. Pan, G. Liu, G. Q. Lu, H.-M. Cheng, *Angew. Chem. Int. Ed.* **2011**, *50*, 2133.
[61] G. Zheng, J. Wang, X. Liu, A. Yang, H. Song, Y. Guo, H. Wei, C. Jiao, S. Yang, Q. Zhu, Z. Wang, *Appl. Surf. Sci.* **2010**, *256*, 7327.
[62] P. M. Kumar, S. Badrinarayanan, M. Sastry, *Thin Solid Films* **2000**, *358*, 122.
[63] D. E. Skinner, D. P. C. Jr, J. J. Cavaleri, R. M. Bowman, *J. Phys. Chem.* **1995**, *99*, 7853.
[64] N. Serpone, D. Lawless, R. Khairutdinov, *J. Phys. Chem.* **1995**, *99*, 16646.
[65] M. Anpo, N. Aikawa, Y. Kubokawa, *J. Phys. Chem.* **1985**, *89*, 5017.
[66] N. Daude, C. Gout, C. Jouanin, *Phys. Rev. B* **1977**, *15*, 3229.
[67] F. Amtz, Y. Yacoby, *Phys. Rev. Lett.* **1966**, *17*, 857.
[68] A. G. Thomas, W. R. Flavell, A. K. Mallick, A. R. Kumarasinghe, D. Tsoutsou, N. Khan, C. Chatwin, S. Rayner, G. C. Smith, *Phys. Rev. B.* **2007**, *75*, 35105.
[69] B. Lin, Z. Fu, Y. Jia, *Appl. Phys. Lett.* **2001**, *79*, 943.
[70] Y. W. Heo, D. P. Norton, S. J. Pearton, *J. Appl. Phys.* **2005**, *98*, 73502.
[71] T. B. Hur, G. S. Jeen, Y. H. Hwang, H. K. Kim, *J. Appl. Phys.* **2003**, *94*, 5787.
[72] J. Wang, P. Liu, X. Fu, Z. Li, W. Han, X. Wang, *Langmuir.* **2009**, *25*, 1218.
[73] Y. Zhang, H. Xu, Y. Xu, H. Zhang, Y. Wang, *J. Photochem. Photobiol. A: Chem.* **2005**, *170*, 279.
[74] J. R. Yu, W. C. Hoi, *Environ. Sci. Technol.* **2008**, *42*, 294.
[75] T. Morikawa, R. Asahi, T. Ohwaki, K. Aoki, Y. Taga, *Jpn. J. Appl. Phys* **2001**, *40*, L561.
[76] M. R. Hoffmann, S. T. Martin, W. Choi, D. W. Bahanemann, *Chem. Rev.* **1995**, *95*, 69.